MODELLING EYE-MOVEMENT CONTROL VIA A CONSTRAINED SEARCH APPROACH

G. Boccignone

Universitá di Milano
Dipartimento di Scienze dell'Informazione
Via Comelico 39/41, Milano, 20135 Italy

M. Ferraro

Universitá di Torino
Dipartimento di Fisica Sperimentale
Via Giuria 1, Torino 10125, Italy

ABSTRACT

A model of visual search is presented where gaze shifts are driven by an hybrid deterministic/stochastic mechanism operating over a saliency field. Results of the simulations are compared with experimental data, and a notion of complexity is used to quantify the behaviour of the system in different conditions.

Index Terms— Eye movements, random walk, active vision, information encoding

1. INTRODUCTION

Visual systems have a limited informational capacity [1], in the sense that only a small part of information present is registered, at any given time, and reaches levels of processing that directly influence behavior; thus, an extensive, search over the whole visual field would be time-consuming and would prevent a fast response to the environmental stimuli. The problem for the organism is to select which part of the scene needs to be attended to, or, in other words, which fraction of information is useful for behavioral purposes and must be processed. Visual attention controls and ensures that selected information is relevant to behavioral priorities and objectives. Kustov and Robinson have suggested that the attentional process evolved as part of the motor system [2] and eye movements are directly related to the capability of the observer for exploring the environment. In particular, overt visual attention, supported by movements of agent's body, head and eyes ensures fast and fluent responses (e.g., detect a predator) to a changing environment.

The visual system of primates achieves highest resolution in the fovea and the brain exploites saccades to actively reposition the center of gaze (fixation) on regions of interest so as to extract detailed information from the visual environment. The succession of gaze shifts is referred to as a scanpath. A scanpath of a subject scanning a natural scene is shown in Fig. 1: circles and lines joining circles, graphically represent, respectively, fixations and gaze shifts between subsequent fixations. Note that different observers (or even the same observer along different trials) could produce slightly different scanpaths, on the same figure, as regards the order in which different regions of interest of the image are visited. The selection of a fixation point, which allows to set the

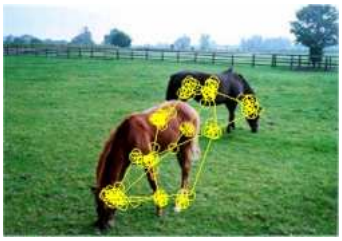

Fig. 1. Scanpath eye-tracked from a human observer, graphically overlapped on the original "Horses" image

observer's focus of attention (FOA) on the foveated region, appears to be driven by two different mechanisms: "bottom up" process which produces rapid scans in a saliency-driven, task-independent manner and a slower "top down" process which is task-dependent and volition-controlled. The degree to which these two mechanisms play a role in determining attentional selection under natural viewing conditions has been for a long time under debate.

In [3], a gaze-shift model (denoted Constrained Levy Exploration, CLE) has been proposed and refined in [4, 5] for robotic applications. Such model is somehow akin to models of simple animal foraging, where the visual system hunts for areas that are rich in visual saliency. In other terms, eye movements and animal foraging address in some way the problem of searching randomly distributed sites whose exact locations are not known a priori. The exploration is guided by a Langevin equation,

$$\frac{d\vec{r}}{dt} = -\vec{\nabla} V(\vec{r}) + \vec{\eta}, \tag{1}$$

where V can be modelled as a function of the saliency (landscape) and $\vec{\eta}$ is a stochastic vector used to sample flight lengths from a Levy distribution. Levy distributions of flight lengths, as opposed, for instance, to Gaussian walk, may be essential for optimal search in foraging, where optimality is related to efficiency, that is the ratio of the number of sites visited to the total distance traversed by the forager [6]. The

model, while accounting for "noisy", idiosyncratic variations of the random exploration exhibited by different observers when viewing the same scene, or even by the same subject along different trials, roughly mimicked a straight reactive behavior of the observer/forager with respect to the potential designed on the basis of landscape saliency. In other term it represented a low-level layer of a complex sensorimotor control module.

However, one could argue, from an evolutionary standpoint, that specific search mechanisms could have been subsequently learned and "wired" in order to improve the exploration reliability and efficiency. For example, it has been suggested [7] that, to optimize the search of the target sites, locomotion rules need to be embedded within the search mechanism.

In the model presented here the process of random search can, under certain conditions on the saliency of the image, be overruled by a simple local deterministic rule, resulting in an hybrid dynamical system (Hybrid Constrained Search, HCS). This process can be seen as the result of the action of a higher-level control system superimposed to the lower stochastic one. This idea is consistent with view, dating back to Jackson's work [8], that the evolution of the nervous system can be seen as an incremental process in which higher-level control systems overrule lower levels, which however are retained and to which control is returned when the interaction of the biological system with the environment does not fulfill appropriate conditions or a breakdown occurs at the higher level. Thus, during ontogeny, (development) the brain matures through the sequential addition of higher centers [9] ; this form of development has been observed post-natally in the maturation of rats and rhesus monkeys [9]. For instance, in rats, reflexive responses to stimuli (visual, auditory, or gustatory) have been shown to mature several days before the same stimuli are able to mediate learned behavioral reactions. Unlearned reflexive responses can be generated by the brainstem components of sensory systems, whereas learned behaviors of this kind generally require higher-level components.

In the following it will be shown that HCS exhibits a more robust behavior with respect to external noise than the simple CLE [3].

2. THE MODEL

Consider an image as a smooth mapping from a domain $D \subseteq \mathbf{R}^2$ to an m-dimensional range, $\vec{f} : D \rightarrow \mathbf{R}^m$; thus the image can be just a scalar field, as in grey-level images, or a vector field, for instance in case of color images, where the three color channels are the vector components (e.g., red green and blue, RGB). Then, a saliency field s upon the image is defined, that is a landscape upon which the visual exploration is performed. Such map $s(\cdot)$ is a scalar field obtained through a transformation $\vec{f} \mapsto s(\vec{f}) \in \mathbf{R}$.

Several approaches have been presented in the literature to derive s fields, based on classical image processing algorithms [10] or biologically motivated processing [11]. For instance Fig. 2 shows the saliency map obtained from the "Horses" image in Fig. 1 using the approach outlined in[11].

Fig. 2. Saliency field obtained from the "Horses" image

This is basically a pure bottom-up process; however, top-down influences can be taken into account either by modifying such weights using a supervised learning algorithm, and/or by increasing the saliency values on connected subdomains of the visual field representing the support for specific region of interest (e.g., faces detected by a specialized face detection module).

At each gaze shift, in order to deal with a fixation dependent (foveated) map, we define a weighted saliency $\hat{s}$ gauged at a fixation center (x_s, y_s) as

$$\hat{s}(x_s, y_s) = \sum_{x,y \in N} s(x, y) \exp(-\frac{(x - x_s)^2 + (y - y_s)^2}{\sigma^2}), \tag{2}$$

where N is the support region (FOA neighborhood) centered at (x_s, y_s) whose dimension is modulated by σ (which experimentally can be set to $1/6$ of the smallest between the input image width or height [11]). Given such preliminary representation, the search strategy can be summarized as follows. First the system detects a candidate target site $\vec{r}_{new}$ that must be located within a "direct vision" distance ρ from the current position $\vec{r}$, according to the rule:

$$\vec{r}_{new} = \arg\max_{\vec{r}'} \{\hat{s}(\vec{r}')\}_{\vec{r}' \in \mathcal{N}_{\vec{r}}}, \tag{3}$$

where $\mathcal{N}_{\vec{r}}$ is the circle of radius ρ centered on $\vec{r}$ and $\vec{r} \neq \vec{r}'$. Denote the saliency gain $\Delta\hat{s}$ as

$$\Delta\hat{s} = \hat{s}(\vec{r}_{new}) - \hat{s}(\vec{r}); \tag{4}$$

if $\Delta\hat{s}$ is larger than a fixed threshold ξ, then the gaze moves directly to the site $\vec{r}_{new}$ which becomes the current fixation point.

On the contrary, if there are no target sites located within a direct vision distance then the system switches to a random search strategy, that amounts to a Levy flight, a random walk with non-local transition probabilities in the saliency field $\hat{s}$

whose steps are generated according to a Levy distribution. The random walk is constrained by the saliency field, and modelled by the Langevin equation. More precisely, write Eq. (1) as

$$\frac{dx}{dt} = -\frac{\partial V(\vec{r})}{\partial x} + \eta_x$$
$$\frac{dy}{dt} = -\frac{\partial V(\vec{r})}{\partial y} + \eta_y. \quad (5)$$

Here V is a decreasing function of the saliency field s,

$$V(x, y) = \exp(-\tau_V s(x, y)), \quad (6)$$

and $\vec{\eta} = (\eta_x, \eta_y)^T$ is a stochastic vector. Fig. 3 shows the V field obtained applying Eq. (6), with $\tau_V = 0.01$, to the saliency map presented in Fig. 2. The stochastic component

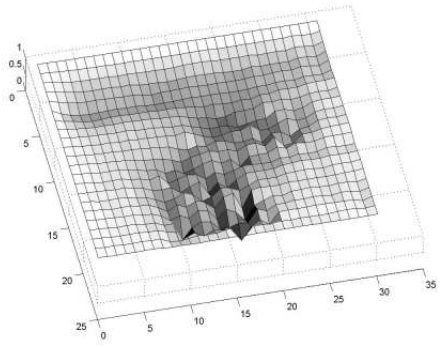

Fig. 3. Potential landscape obtained from the saliency map shown in Fig. 2

$\vec{\eta}$ in equation (5) is generated by a modified Cauchy-Levy distribution. Set

$$\eta_x = l\cos(\alpha),$$
$$\eta_y = l\sin(\alpha), \quad (7)$$

where the angle α represents the flight direction randomly chosen according to a uniform distribution in the $[0, 2\pi]$ interval; the jump length l is obtained from the weighted Cauchy-Levy distribution:

$$p(l) = \frac{D\varphi(s)}{l^2 + D^2}. \quad (8)$$

The function $\varphi(s)$ modifies the pure Levy flight, in that the probability $p(\vec{r}_{new} \mid \vec{r})$ to move from a site $\vec{r}$ to the next site $\vec{r}_{new}$ depends on the "strength" of a bond φ that exists between them [12] . Thus, the jump has a higher probability to occur if the target site is strongly connected in terms of saliency; for any pair $(\vec{r}, \vec{r}_{new})$, $\varphi(s)$ is chosen as

$$\varphi(s) = \frac{\exp(-\beta_P(s(\vec{r}) - s(\vec{r}_{new})))}{\sum_{\vec{r}'_{new}} \exp(-\beta_P(s(\vec{r}) - s(\vec{r}'_{new})))} \quad (9)$$

where $\vec{r}$ and $\vec{r}_{new}$ represent the present site and the target site respectively, $\vec{r}'_{new}$ ranges over the set of candidate targets.

Next, the jump length l, computed according to Eq. (8), undergoes an acceptance process, implemented by a Metropolis algorithm [13]: the flight is accepted according to a probabilistic rule that depends on the gain of saliency and on a "temperature" T, whose values determine the amount of randomness in the acceptance process. Thus, the target site $\vec{r}_{new}$ is accepted with probability

$$p(a|\vec{r}_{new}, \vec{r}) = \min\{1, \quad \exp(\Delta\hat{s}/T)\} \quad (10)$$

It should be remarked that the stochastic process has been subdivided in two steps - flight generation and acceptance of the new site - for simplicity's sake, and these two steps together provide a rough computational approximation of a highly complex sensory-motor process, which is far from being fully understood [14].

The exploration of the visual field performed according to the rules of selection described above, can be summarized in the following *Hybrid Constrained Search algorithm*:

Compute the saliency map $s(\cdot)$ of the image
Compute potential V according to Eq. (6)
Compute φ through Eq. (9)
$\vec{r} \leftarrow$image center; $n \leftarrow 0$
repeat
  Current fixation$\leftarrow \vec{r}$, accepted$\leftarrow false$
  $\vec{r}_{new} \leftarrow \arg\max_{\vec{r}}\{s(\vec{r}')\}_{\vec{r}' \in \mathcal{N}_{\vec{r}}}$
  Compute $\Delta\hat{s} = \hat{s}(\vec{r}_{new}) - \hat{s}(\vec{r})$
  if $\Delta\hat{s} > \xi$ **then**
    Store $\vec{r}_{new}$; $\vec{r} \leftarrow \vec{r}_{new}$; accepted$\leftarrow true$; $n \leftarrow n+1$
  while not accepted **do**
    Generate randomly a jump length l, in a random direction α, with probability $p(l)$ drawn according to Eq.(8)
    Compute $\vec{r}_{new}$ via Langevin equation (5)
    Compute $\Delta\hat{s} = \hat{s}(\vec{r}_{new}) - \hat{s}(\vec{r})$
    if $\Delta\hat{s} > 0$ **then**
      Store $\vec{r}_{new}$; $\vec{r} \leftarrow \vec{r}_{new}$; accepted$\leftarrow true$; $n \leftarrow n+1$
    else
      Generate a random number ρ
      if $\rho < \exp(\Delta\hat{s}/T)$ **then**
        Store $\vec{r}_{new}$; $\vec{r} \leftarrow \vec{r}_{new}$; accepted$\leftarrow true$; $n \leftarrow n+1$
until $n \leq K$

3. SIMULATION AND DISCUSSION

Results from HCS, obtained by solving Eq. (5) through a finite difference scheme with reflecting boundary conditions are shown in Fig. 4 and should be compared with those presented in Fig. 1 and those obtained by the CLE algorithm [3] (Fig. 5).

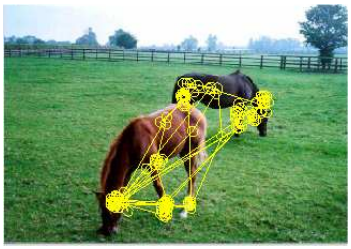

Fig. 4. Scanpath obtained using the HCS algorithm, graphically overlapped on the original "Horses" image

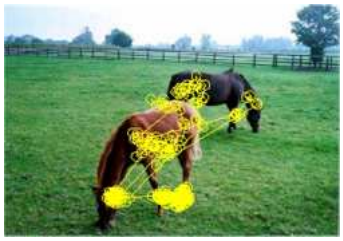

Fig. 5. Scanpaths obtained using the CLE algorithm

The jump length probability, Eqs. (8) and (9), were generated with $\beta_P = 1.0$ and $D = 0.8$; in both images shown in Figs. 4 and 5 $K = 10000$ and $T = 2.0$, $T = 1.5$ for the HCS and CLE algoritms, respectively.

Consider now images presented in Figs. 6 and 7, together with those presented in Figs. 4 and 5: they show that for increasing T, three kinds of behavior basically occur. In a first low-temperature range, the exploration is trapped in some local potential (left images of Figs. 6 and 7) , while a subsequent range provides normal scanpaths (such as those shown in Figs. 1,4 and 5), and a high-temperature range gives rise to an unconstrained walk (right images of Figs. 6 and 7). Scanpaths of human observers, then, are situated somewhere in the middle between two extreme cases [3].

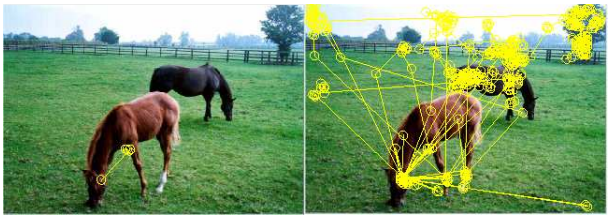

Fig. 6. Scanpath obtained applying the HCS algorithm at $T = 0$, $T = 15$ (left and right images, respectively)

However, note the different behaviors of the two algorithms for increasing T: it can be appreciated that the HCS method provides a more stable behavior with respect to the CLE one. Such a behavior can be given a more precise characterization by introducing a measure of complexity.

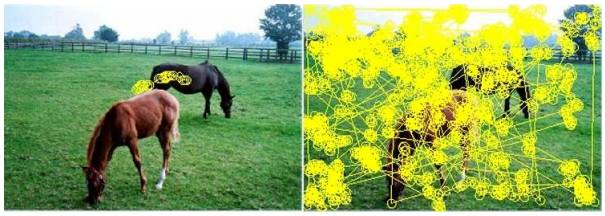

Fig. 7. Scanpath obtained applying the CLE algorithm at $T = 0$, $T = 15$ (left and right images, respectively)

3.1. Scanpath complexity

Consider the probability distribution p_m derived as follows. First suppose to subdivide the image into N windows and let $p(i)$ be the probability that the gaze is at window i when $t \to \infty$, in other words $p(i)$ is the asymptotic probability distribution. Subregion partitioning of the image, which performs a coarse-graining of the states the gaze can take, is justified by the fact that gaze-shift relevance is determined according to the clustering of fixations that occur in a certain region of the image, rather than by single fixations [10]. Thus, the image was partitioned into $N = 16$ rectangular $n \times m$ windows $w(x_i, y_i)$. For all K fixations, each fixation occurring at $\vec{r}_k = (x, y)$, $k = 1 \dots K$, was assigned to the corresponding window, and probability $p(i)$ was empirically estimated as

$$p(i) \simeq \frac{1}{K} \sum_{k=1}^{K} \chi_{k,i} \tag{11}$$

where $\chi_{k,i} = 1$ if $\vec{r}_k \in w(x_i, y_i)$ and 0 otherwise.

The corresponding Boltzmann-Gibbs-Shannon entropy is $S = -k_B \sum_{i=1}^{N} p(i) \log p(i)$. In the sequel, the Boltzmann's constant is set $k_B = 1$. The supremum of S is obviously $S_{sup} = \ln N$ and it is associated to a completely unconstrained process, that is a process where $s = const$, since with reflecting boundary conditions the asymptotic distribution is uniform. Furthermore S is a monotonically increasing function of T since for $T \to \infty$ the scanpath tends to cover uniformally the whole image and hence $\lim_{T\to\infty} p(a|\vec{r}_{new}, \vec{r}) = 1$.

Define, following [15], a disorder parameter Δ as $\Delta \equiv S/S_{sup}$ and an order parameter Ω as $\Omega = 1 - \Delta$; complexity Γ is given by

$$\Gamma = \Delta\Omega, \tag{12}$$

which ideally is a concave function of T, $\Gamma \approx 0$ for both completely ordered and completely disordered systems, and a has a maximum at some intermediate order/disorder ratio.

As mentioned earlier the model accounts for "noisy", idiosyncratic variations of the random exploration exhibited by different observers when viewing the same scene, or even by the same subject along different trials. Thus, we can think

of each scanpath generated by the model as a single observation. To characterize the behavior of the system, we compute the average complexity $< \Gamma >= \frac{1}{N}\sum_{n=1}^{N}\Gamma_n$, where Γ_n is the complexity of the n-th trial at a fixed temperature T.

The average complexity $< \Gamma >$ of scanpaths, as a function of T, is depicted in Figs. 8 (a) and (b) that show $< \Gamma >$ computed on the "Horses" image, by using HCS and CLE algorithms,respectively, for increasing temperatures in the range $[0, 30]$, and $N = 50$ trials at each T, the other parameters being the same used to obtain images in Figs. 5, 4.

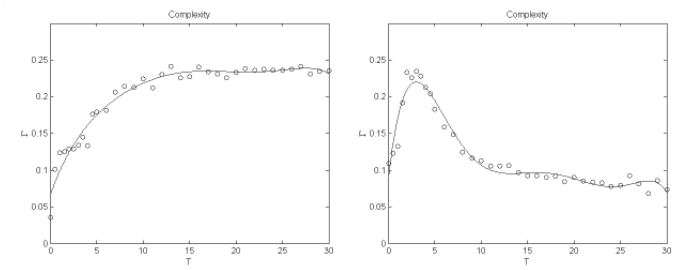

(a) HCS algorithm (b) CLE algorithm

Fig. 8. Average complexity curve for the "Horses" image obtained using the HCS algorithm (a) and using the CLE algorithm (b)

By considering a purely random exploration (CLE model), it can be observed (Fig. 8) how, in a first low-temperature range, the search is mainly affected by the local potential and is trapped at local minima of V and hence $< \Gamma >$ is low. When T increases (typically, $T > 1$), the random force becomes more effective in driving the search and scanpath are generated, which are similar to those obtained by human observers; finally, at "temperatures" higher than $T = 10$ the process appears to be driven by the stochastic component and practically unaffected by the saliency of different image regions.

Conversely, the behavior of $< \Gamma >$ in case of hybrid rule-based /random exploration (HCS model, Fig. 8(a)) suggests that the average observer's behavior becomes more robust with respect to variations of temperature T, because coded rules somehow contrast the random component of the search.

Further, this robustness can be more precisely accounted in terms of the informational divergence of the system with respect to the behavior of a normal viewer. Namely, consider again probability $p(i)$ estimated according to Eq. (11), and apply this procedure both to experimental results and to data generated by the model at different temperatures T; corresponding probabilities are denoted by p_h, p_m, respectively. Next, the divergence, or distance J can be computed [16],

$$J = \sum_{k=1}^{K}(p_h(k) - p_m(k)) \ln \frac{p_h(k)}{p_m(k)}, \qquad (13)$$

which is used in information theory to quantify the difference between two probability distributions, and in particular has been applied to target recognition issues. The divergence J, which is obviously a function of T, represents the distance between the model prediction and the experimental data, and we denote $< J(T) >$ the average divergence computed over different runs of the simulation.

The average divergence $< J(T) >$ of model scanpaths with respect to the human generated one, as a function of T, is depicted in Figs. 9 (a) and (b). The figures plot $< J(T) >$ computed on the "Horses" image, by using HCS and CLE algorithms, respectively, for increasing temperatures in the range $[0, 30]$, and $N = 50$ trials at each T, the other parameters being the same used to obtain images in Figs. 5, 4.

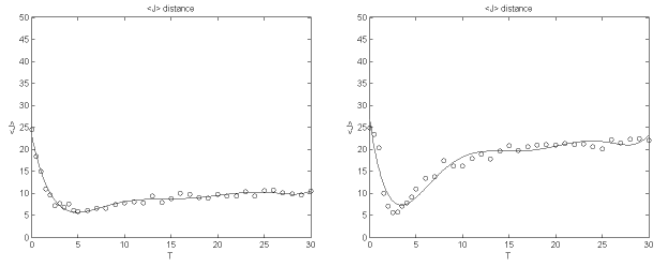

(a) HCS algorithm (b) CLE algorithm

Fig. 9. Average divergence curve for the "Horses" image obtained using the HCS algorithm (a) and using the CLE algorithm

From Figs. 9 (a) and (b) it can be seen that the observer's behavior, when modelled through the layered system (HCS), exhibits a high level of performance for different values of T, rather than a single peak of performance as in case of CLE, resulting thus more robust with respect internal/external noise. It should also be noted that in the case of HCS the system exhibit a higher "computational efficiency", in the sense that when a very salient point is available at a glance, random search is avoided, thus lowering the computational complexity of the search, which in turn corresponds to a an increased reactivity to environmental stimuli. Summing up, the development of a simple higher level control upon an existing lower level one, may endow the biological system with more reliable and fast responses to the surrounding environment.

4. CONCLUSIONS

The results presented here make clear that the addition of deterministic rules result in more efficient and robust processes of visual exploration. In this sense the layered organization of the HCS system provides a better model of human gaze-shift behavior than CLE, in that humans appear able to perform an efficient scanpath under different environmental conditions. A layered architecture as organizing principle of the vertebrate brain has also interesting parallels with Brooks' subsumption architectures for the control of artificial creatures [17]. Even though HCS relies upon a bottom-up search, it can, in principle, be modified to deal with the case of top down vision. For instance rather than looking for a point with large saliency values the model could be amended to give priority to fixations at regions representing objects that have relevance in determining organism behavioral responses. Interestingly enough, for a broad range of T values the system is able to perform normally, whereas very small and very large T values may correspond to pathological viewing conditions. For instance if T is very low the system simulates a disengagement deficit, as in Alzheimer's syndrome [18], whereas higher temperatures account for impairments of saccadic control as occur in Parkinson's disease, schizophrenia, hyperactivity or autistic behaviors [19]

.

5. REFERENCES

[1] P.S. Churchland, VS Ramachandran, and T.J. Sejnowski, *A Critique of Pure Vision*, The MIT Press, 1994.

[2] AA Kustov and DL Robinson, "Shared neural control of attentional shifts and eye movements.," *Nature*, vol. 384, no. 6604, pp. 74, 1996.

[3] G. Boccignone and M. Ferraro, "Modelling gaze shift as a constrained random walk," *Physica A: Statistical Mechanics and its Applications*, vol. 331, no. 1-2, pp. 207–218, 2004.

[4] H. Martinez, M. Lungarella, and R. Pfeifer, "Stochastic Extension to the Attention-Selection System for the iCub," *University of Zurich, Tech. Rep*, 2008.

[5] Y. Nagai, "From bottom-up visual attention to robot action learning," in *Proceedings of 8 IEEE International Conference on Development and Learning*. IEEE Press, 2009.

[6] GM Viswanathan, F. Bartumeus, S. V. Buldyrev, J. Catalan, UL Fulco, S. Havlin, MGE Da Luz, ML Lyra, EP Raposo, and H. Eugene Stanley, "Levy flight random searches in biological phenomena," *Physica A: Statistical Mechanics and Its Applications*, vol. 314, no. 1-4, pp. 208–213, 2002.

[7] MGE Da Luz, S.V. Buldyrev, S. Havlin, EP Raposo, H.E. Stanley, and GM Viswanathan, "Improvements in the statistical approach to random Lévy flight searches," *Physica A: Statistical Mechanics and its Applications*, vol. 295, no. 1-2, pp. 89–92, 2001.

[8] JH Jackson, "Evolution and dissolution of the nervous system (Croonian Lectures). Published in parts in the," *British Medical Journal, Lancet*, pp. 5–75, 1958.

[9] J.W. Rudy, S. Stadler-Morris, and P. Albert, "Ontogeny of Spatial Navigation Behaviors in the Rat: Dissociation of," *Behavioral Neuroscience*, vol. 101, no. 1, pp. 62–73, 1987.

[10] C. M. Privitera and L. W. Stark, "Algorithms for defining visual regions-of-interest: Comparison with eye fixations," *IEEE Trans. Pattern Anal. Machine Intell.*, vol. 22, no. 9, pp. 970–982, September 2000.

[11] L. Itti, C. Koch, and E. Niebur, "A model of saliency-based visual attention for rapid scene analysis," *IEEE Trans. Pattern Anal. Machine Intell.*, vol. 20, pp. 1254–1259, 1998.

[12] M.A.P. Idiart and M. Trevisan, "Directing a random walker with optimal potentials," *Physica A: Statistical Mechanics and its Applications*, vol. 307, no. 1-2, pp. 52–62, 2002.

[13] N. Metropolis, A.W. Rosenbluth, M.N. Rosenbluth, A.H. Teller, E. Teller, et al., "Equation of state calculations by fast computing machines," *The journal of chemical physics*, vol. 21, no. 6, pp. 1087, 1953.

[14] R.J. Krauzlis and L.S. Stone, "Tracking with the mind's eye," *Trends Neuroscience*, vol. 22, no. 12, pp. 544–550, 1999.

[15] JS Shiner, M. Davison, and PT Landsberg, "Simple measure for complexity," *Physical review E*, vol. 59, no. 2, pp. 1459–1464, 1999.

[16] D. Sheffer and D. Ingman, "The informational difference concept in analyzing target recognition issues," *JOSA A*, vol. 14, no. 7, pp. 1431–1438, 1997.

[17] R.A. Brooks, "New approaches to robotics," *Science*, vol. 253, no. 5025, pp. 1227, 1991.

[18] A. Jones, RP Friedland, B. Koss, L. Stark, and BA Thompkins-Ober, "Saccadic intrusions in Alzheimer-type dementia," *Journal of neurology*, vol. 229, no. 3, pp. 189–194, 1983.

[19] B.A. Clementz and J.A. Sweeney, "Is eye movement dysfunction a biological marker for schizophrenia? A methodological review," *Psychological Bulletin*, vol. 108, no. 1, pp. 77–92, 1990.